Published in : Macromolecular Chemistry and Physics (2025), vol. 226, n°21, e00242
DOI: 10.1002/macp.202500242
Status : Postprint (Author's version)

COMPOSITE POLYMER ELECTROLYTES BASED ON SILICON DIOXIDE NANOPARTICLES FOR LITHIUM METAL BATTERIES

Ashish Raj

Institute of Condensed Matter and Nanoscience (IMCN), Louvain-la-Neuve, Belgium

Bruno Grignard

Center For Education and Research on Macromolecules (CERM), CESAM Research Unit, University of Liège, Liège, Belgium – Federation of Researcher in Innovation Technologies For CO_2 Transformation (FRITCO2T Research Platform), University of Liège, Liège, Belgium

Maxime Bourguignon

Center For Education and Research on Macromolecules (CERM), CESAM Research Unit, University of Liège, Liège, Belgium

Christophe Detrembleur

Center For Education and Research on Macromolecules (CERM), CESAM Research Unit, University of Liège, Liège, Belgium – WEL Research Institute, Wavre, Belgium

Jean-François Gohy

Institute of Condensed Matter and Nanoscience (IMCN), Louvain-la-Neuve, Belgium

Funding: The author received no specific funding for this work.

Keywords: electrolyte | interface | lithium metal battery | poly(hydroxyurethane) | SiO_2

ABSTRACT

Composite polymer electrolytes (CPEs) formed of non-ionically conducting inorganic fillers, such as SiO_2 nanoparticles, dispersed in a polymer matrix, are considered as promising candidates for solid-state lithium metal batteries. By decreasing the crystallinity and lowering the T_g of the polymer matrix, and inducing Lewis acid-base interactions with lithium salts, inorganic fillers are reportedforincreasingiontransportinCPEs.Here,wedisclosetwotypesofcompositepolymerelectrolytes(CPEs).ThefirstCPEis a blend comprising lithium salt-loaded poly(ethylene oxide) (PEO) as polymer matrix, bio-based carbonated soybean oil (CSBO) as additive, and SiO_2 nanoparticles as inorganic component. The second CPE is a lithium salt-loaded poly(hydroxyurethane) network

Published in : Macromolecular Chemistry and Physics (2025), vol. 226, n°21, e00242
DOI: 10.1002/macp.202500242
Status : Postprint (Author's version)

prepared from α,ω-diamino PEO and CSBO cross-linker as polymer matrix entrapping SiO_2 nanoparticles. For both CPEs, the combined effect of the polymer component and SiO_2 facilitates the formation of electrolyte membranes with good flexibility and conductivity in the range of 10^{-5} S cm^{-1} at 60°C. Moreover, the addition of inorganic fillers broadens oxidative potential limitations to > 4.8 and 4.4 V versus Li/Li^+ for CPEs based on linear PEO and PHU network polymers, respectively. Finally, the PEO-CSBOSiO_2-based LFP-Li cell delivers an interesting initial discharge capacity of 140 mAh g^{-1} at 0.1C and 60°C.

1. Introduction

The clean energy transition stresses higher energy density needs and mass grid storage. Over the last two decades, lithium ion batteries (LiBs) have dominated the battery market with higher projections and a surge in electric vehicles demand. In this context, safe and superior-performing batteries bet on the utilization of solid-state electrolytes with high-capacity electrodes owing to their lightweight, robust flexibility, easy stacking, and cost-effectiveness [1, 2]. Conventional liquid electrolytes pose issues like leakage, decomposition, and flammability [3]. One of the major reasons behind the solid-state electrolyte push is the utilization of lithium metal for its high capacity (3860 mAh g^{-1}), energy density of ca. 250 Wh Kg^{-1} and high oxidation potential limitations [1, 4]. However, solid-state electrolytes present their own challenges involving high electrolytic and interfacial resistance, which limit their application. To tackle those issues, several approaches are being carried out, from designing novel materials, processing of materials, and interfacial understanding and engineering. In this respect, the working and failure mechanisms analysis via theoretical and experimental approaches has become equally relevant due to their high complexities [2, 5– 7]. Although most of the works have focused on the interfacial engineering between solid-state electrolytes and electrodes, the control of interfaces inside solid-state electrolytes and electrodes has become equally important. Several recent reviews have summarized interfacial problems in solid-state batteries and strategies to tackle them [8, 9].

Over several years of research, it has been considered that a hybrid electrolyte proffers more potential prospects than a solid polymer electrolyte (SPE) and an inorganic solid electrolyte (ISE) alone. In theory, a hybrid electrolyte, formed by blending various amounts of ISE and SPE, combines superior ionic conductivity, oxidation stability, and lower thermal degradation with higher interfacial, mechanical, and cost-effective merits compared to the starting ISE and SPE [10, 11]. The ionic conductivity in SPE is usually credited to ion hopping from one polar group to another, largely via oxygen coordination and polymer chain segmental motion, in particular for polymers above their glass transition temperature (T_g) [12, 13]. While in ISE, the ion transport mechanism is more complex than in SPE and usually takes place via defects such as Schottky and Frenkel defects involving vacancies and interstitial locations for hopping [13–15]. Based on the type of hybrid electrolytes, different principles are applied, and thus the mechanism of the lithium ions pathway varies from the newly proposed paddle wheel model to grain boundaries resistance. However, the hypothesized ion pathways are very often perturbed by

Published in : Macromolecular Chemistry and Physics (2025), vol. 226, n°21, e00242
DOI: 10.1002/macp.202500242
Status : Postprint (Author's version)

passivation layers formed at the interface between the ISE and SPE components, hindering efficient transport of lithium ions between both partners.

Composite polymer electrolytes (CPEs) in which non-ionically conducting inorganic fillers are dispersed in a polymer matrix are substantially different from the hybrid electrolytes described above. Passive fillers, such as SiO_2, Al_2O_3, ZnO, TiO_2, etc, usually decrease or even suppress the crystallinity and lower the T_g of the polymer matrix. This further enhances the mobility of charge carriers. However, the physical interaction between the different phases in CPEs could promote the agglomeration of fillers, resulting in an increased interfacial impedance and a decreased ionic conductivity of the electrolyte [8]. In addition, they induce Lewis acid-base interactions with lithium salts in the CPE [16, 17]. As a result, salt dissociation is improved along with segmental motion and ion transport. Several reports on CPEs based on silicon dioxide (SiO_2) have shown potential outcomes. Especially, nano-sized silicon dioxide particles due to their size, stability, and cost-effectiveness, are a lucrative choice. As a typical example, Cai and coworkers reported poly(ethylene oxide) (PEO) Li salt based CPEs with embedded SiO_2 particles further soaked in ethylene carbonate/propylene carbonate to form a gel electrolyte [17]. Particles with different nanostructures and morphology, like nanowires, 3D spheres, and mesoporous structures, have been investigated and show high compatibility with polymers, demonstrating conductivities in the range of 10^{-4}–10^{-5} S cm^{-1} at room temperature [18–20]. Among other approaches, functionalization of SiO_2 nanoparticles has also been explored as a smart method to develop beneficial interactions between nanoparticles and polymer functional groups. For example, a cross-linked composite gel polymer electrolyte was prepared with mesoporous SiO_2 nanoparticles containing reactive methacrylate groups as cross-linking sites and dispersed into a fibrous polyacrylonitrile membrane [21].

Most of the previous investigations are largely based on PEO or similar functional polymers, while there are very few reports on passive or active fillers incorporated into polyurethanes/poly(hydroxyurethane)s (PUs/PHUs), which are however looked upon as potential polymer electrolytes owing to their functional groups exhibiting a dual nature of conductivity and mechanical properties. As a typical example, Zhang et al. prepared a hybrid electrolyte by combining linear PU and $Li_{0.35}La_{0.55}TiO_3$ (LLTO) ion conducting particles, which exhibited a high conductivity of 3.8 × 10^{-4} S cm^{-1} at ambient temperature [22].

In the pursuit of sustainable CPEs, we investigate here the effect of an inexpensive passive filler, SiO_2, embedded into PEO blended with carbonated soybean oil (CSBO), or into a PHU network originated from CSBO and PEO-based diamines. We intend to demonstrate the synergetic effect of SiO_2 and CSBO or PHU in terms of conductivity and other characteristic properties. Several formulations have been analyzed with SiO_2 filler and lithium bis(trifluoromethanesulfonyl)imide as lithium salt for an optimum CPE compatible with lithium metal.

Published in : Macromolecular Chemistry and Physics (2025), vol. 226, n°21, e00242
DOI: 10.1002/macp.202500242
Status : Postprint (Author's version)

2. Experimental Section

2.1. MATERIALS AND METHODS

4,7,10-Trioxa-1,13-tridecanediamine (TTD) (MW ≈ 220.31 g mol^{-1}), silicon dioxide (SiO_2, spherical nanoparticles with diameter ≈ 10–20 nm), anhydrous tetrahydrofuran, battery-grade lithium, lithium bis(trifluoromethanesulfonyl)imide (LiTFSI) and PEO (MW ≈ 10^6 g mol^{-1}) and silicon dioxide nanopowder (10–20 nm particle size) were purchased from Sigma–Aldrich. Bis(3-aminopropyl) terminated poly(ethylene glycol) (PEGTA) (MW ≈ 1500 g mol^{-1}) was bought from Acros. Carbonated soybean oil (CSBO) was prepared as highlighted in a previous report [23]. Lithium metal foil (99.9%), lithium iron phosphate ($LiFePO_4$), poly(vinylidene fluoride), and super-P carbon were purchased from TOB chemicals. N-methyl-2-pyrrolidone (NMP) was bought from Alfa Aesar. Deuterated chloroform ($CDCl_3$) used for NMR spectroscopy was purchased from Eurisotop. All reactants were used as received, without any further purification.

2.2. CHARACTERIZATION TECHNIQUES

2.2.1. FOURIER TRANSFORM INFRARED SPECTRA (FTIR) MEASUREMENTS

FTIR measurements were carried out on a Nicolet IS5 spectrometer (Thermo Fisher Scientific) equipped with a diamond attenuated transmission reflectance (ATR) device. 32 scans were recorded for each sample for different batches over the range of 4000–500 cm^{-1} with a normal resolution of 4 cm^{-1} and spectra were analyzed with the ONIUM software.

2.2.2. DIFFERENTIAL SCANNING CALORIMETRY (DSC)

DSC analysis was carried out on a Q1000 TA Instruments using standard aluminum pans, calibrated with indium, and nitrogen was used as a purge gas. The samples were analyzed at a heating rate of 10°C min^{-1} over a temperature range from −80 to 200°C under N_2 atmosphere, and the analysis was repeated three times. The degree of crystallization χ_c of PEO segments in the investigated samples is calculated by $\chi_c = (\Delta H_m)/(\omega \times \Delta H_0)$, wherein ΔH_m (J g^{-1}) is the specific heat of fusion, from the integration of the T_m peak from the DSC curve; ΔH_0 (J g^{-1}) is the enthalpy of fusion of 100% crystallinePEO, 205Jg^{-1}; ω is the mass fraction of PEO in the composite material.

2.2.3. THERMOGRAVIMETRIC ANALYSIS (TGA)

TGA was carried out using a Q500 from TA Instruments. Thermal degradation of samples was measured at a heating rate of 20°C min^{-1} over the temperature range of 0–600°C under a N_2 atmosphere.

Published in : Macromolecular Chemistry and Physics (2025), vol. 226, n°21, e00242
DOI: 10.1002/macp.202500242
Status : Postprint (Author's version)

2.2.4. X-RAY PHOTOELECTRON SPECTROSCOPY (XPS)

XPS was performed using an SSI X-Probe (SSX 100/206) photoelectron spectrometer from Surface Science Instruments equipped with a monochromatized Al Kα (200 W) X-ray source. The batteries were disassembled, and samples were mounted on an XPS sample holder in a glovebox prior to transferring to the XPS vacuum chamber in the flux of argon atmosphere. All binding energies were calculated according to the C– (C, H) component of the C1s peak fixed at 284.8 eV. Data analysis was carried out using the CasaXPS software. For the survey scan, a 1.0 eV step size was used, and a 0.1 eV step size was utilized for high-resolution scans for all elements with 150 energy steps.

2.3. ELECTROCHEMICAL ANALYSIS

All electrochemical analyses were carried out on Biologic BCS-COM and VMP3 multichannel potentiostats using CR2032 coin cells.

2.3.1. POTENTIOSTATIC ELECTROCHEMICAL IMPEDANCE SPECTROSCOPY (PEIS)

Ionic conductivity of SPEs was determined by PEIS for symmetric stainless steel (SS|SE|SS) coin cells in the frequency range of 7– 50 MHz, with applied single sinusoidal A.C. excitation voltage of 10 mV. The temperature dependence measurements were carried out from 20°C to 100°C by gradually increasing the temperature at the rate of 0.33°C min^{-1}. One hour was waited between each measurement to reach an equilibrium state. The experiments were repeated for at least three different cells over different batches to avoid any errors.

2.3.2. LINEAR SWEEP VOLTAMMETRY (LSV)

Measurements were performed at various temperatures on an asymmetric CR2032 coin cell as (Li|SPE|Al) over the potential range of 0–6.5 V (vs. Li/Li^+) at the scan rate of 0.5 mV s^{-1} at 60°C over at least three times.

2.3.3. STRIPPING AND PLATING

The symmetric cell, Li|SPE|Li was fabricated for stripping and plating analysis. The cells were charged and discharged for 1 h each for multiple cycles with the variable current densities and cut-off voltage of +4 and −4 V at room temperature under ambient atmosphere using BioLogic BCS-COM multichannel potentiostat.

2.3.4. GALVANOSTATIC CYCLING POTENTIAL LIMITATION (GCPL)

Galvanostatic charge–discharge cycling and rate capabilities measurements for the LFP|SPE |Li cells were tested for various batches of SPEs at different temperatures. The slurries for the cathodes were prepared from $LiFePO_4$, Super P, PVDF, and NMP via grinding using a mortar pestle and were further cast on carbon-coated Al foils using the doctor-blade technique. The coated slurries were then dried

Published in : Macromolecular Chemistry and Physics (2025), vol. 226, n°21, e00242
DOI: 10.1002/macp.202500242
Status : Postprint (Author's version)

in an air oven for more than 6 h at 60°C prior to vacuum drying at 120°C for more than 24 h, leading to cathodes with a typical thickness of 200 micrometers. The cathode components were maintained in the weight ratio of 7:2:1 for LFP, Super P, and PVDF, respectively. The cathodes and anodes were cut into disks of 14 mm in diameter and 16 mm in diameter for the electrolyte membranes.

2.4. SYNTHESIS

2.4.1. SYNTHESIS OF CSBO-PEO-SiO_2

Bio-based cyclic carbonated soybean oil (CSBO) was synthesized by coupling CO_2 to epoxidized soybean oil (ESBO) as reported elsewhere [23]. CSBO-PEO-SiO_2 was prepared by mixing CSBO, PEO, and SiO_2 in various formulations (CSBO:PEO:SiO_2 = x:y:z wt.%) in a vial using acetonitrile as solvent (see Scheme 1). The mixture was stirred for > 6 h and then drop cast on a Teflon mold and later transferred to the vacuum oven. It was maintained at 70°C for ≥ 24 h in a dynamic vacuum and stored in a glove box. For the sake of comparison, CSBO-PEO blends without SiO_2 were also prepared using the same experimental protocol. The CSBOPEO-SiO_2 CPE was prepared following a similar procedure with LiTFSI added to the mixture prior to solvent evaporation.

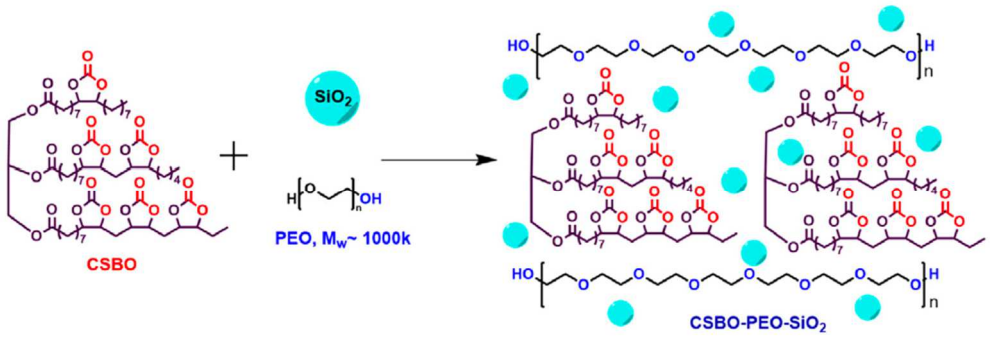

SCHEME 1 | Preparation of blends of CSBO, PEO, and SiO_2 (LiTFSI is not included for the sake of clarity).

2.4.2. SYNTHESIS OF POLY(HYDROXYURETHANE) COMPOSITE (PHU-N2N3-SIO2)

For PHU-N2N3, a ring-opening reaction of the CC groups of CSBO by the amino groups of PEGTA and TDD was conducted with SiO_2 (See Scheme 2). The stoichiometric ratio of TDD (N2) and PEGTA (N3) to CSBO was fixed at 3:1 mol/mol, corresponding to the theoretical opening of the 6 CC rings present on CSBO. While the TDD/PEGTA stoichiometric ratio was set to 3:1 mol/mol. In a typical experiment, 90 mg of CSBO, 81 mg of PEGTA, and 35.69 mg of TDD were taken in a small vial with SiO_2 (5 to 20 wt.% with respect to total monomer wt.%). These were dissolved with anhydrous THF via magnetic stirring at RT for >6 h. The resulting solution was then drop cast on a Teflon mold, followed by transfer to the vacuum oven. The temperature of the vacuum oven was set at 70°C for >12 h and later increased to 90°C for >24 h with dynamic vacuum mode. For the sake of comparison, PHU-N2N3 without SiO_2 was

Published in : Macromolecular Chemistry and Physics (2025), vol. 226, n°21, e00242
DOI: 10.1002/macp.202500242
Status : Postprint (Author's version)

also prepared using the same experimental protocol. A similar procedure was followed for PHU N2N3-SiO_2 CPE with LITFSI added to the initial mixture.

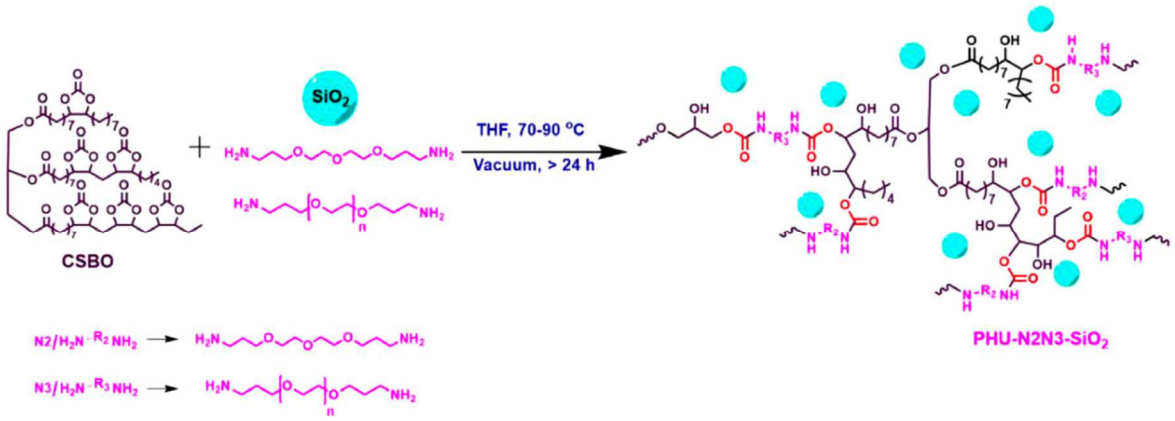

SCHEME 2 | Reaction pathway of PHU-N2N3 formation with SiO_2 nanoparticles (LiTFSI is not included for the sake of clarity).

2.4.3. PREPARATION OF COMPOSITE POLYMER ELECTROLYTE FILMS (CPES)

As indicated above, LiTFSI was added to the mixture prior to blending and curing. The obtained CPE films were peeled off the Teflon molds and stored in the glove box prior to testing. The thickness of the membrane was recorded to be in the range of 50–250 μm for CBSO-PEO-SiO_2 and 100–200 μm for PHU-N2N3-SiO_2, respectively. 2032-type coin cells were assembled using 16 mm punched electrolyte membranes sandwiched between SS|SS, SS|Li, Al-C|Li, and Li|LFP electrode configurations to evaluate electrochemical properties.

3. Results and Discussion

3.1. SYNTHESIS OF CPES

The challenge of improving the properties of SPEs by combining polymers and inorganic fillers seems easier than reality due to various constraints, including intermolecular interactions and granular boundary interfaces. One of the key issues faced among the CPEs is the inhomogeneous distribution of the inorganic particles. This is usually tackled by processing the sample using an extruder, blender, etc. However, the types of polymers, fillers, and salts, along with their concentration and preparation method, play an equally important role. Here, we screen out two different types of polymers, yet related, further incorporated in CPEs based on the same SiO_2 nanoparticles as passive fillers. The first strategy relies on the preparation of CSBO-PEO-SiO_2-LiTFSI blends by a solvent casting method, as shown in Scheme 1. This scheme demonstrates the blending of CSBO, SiO_2, LiTFSI, and PEO, with speculation of the former three entities entrapped within PEO chains constituting the polymer matrix.

Published in : Macromolecular Chemistry and Physics (2025), vol. 226, n°21, e00242
DOI: 10.1002/macp.202500242
Status : Postprint (Author's version)

CSBO molecules and SiO_2 nanoparticles are used here as two distinct plasticizers for the PEO chains, with the double aim to increase PEO chain segment mobility and to decrease PEO crystallinity degree, both factors being expected as boosters for the ionic conductivity of the accordingly obtained SPEs. We have previously disclosed the plasticizing effect of CSBO on PEO-based SPEs [24]. With higher loading of SiO_2 (wt.%), we observed that the CPE films became less transparent and adhesive to the surface (adhesion is contributed by the viscous nature of CSBO), and that a low amount of SiO_2 has to be incorporated to obtain a homogeneous dispersion of those nanoparticles and optimal properties for the SPE membrane (See Figure S1 and Table S1).

In the second approach, we assimilated the SiO_2 filler into a PHU-N2N3 network resulting from the ring-opening reaction of CSBO with a PEO terminated at both ends with amino groups, as depicted in Scheme 2. Two α,ω-diamino PEOs have been blended (N2 and N3) to obtain the PHU-N2N3 network. The N2 molecule is not strictly speaking a polymer but an oligo(ethylene glycol) derivative containing only three ethylene oxide units. It has been selected in order to increase the cross-linking density in the network. While N3 is a α,ω-diamino PEO affording flexibility to the network and a significant number of ethylene oxide to promote lithium ions mobility via an ion-hopping mechanism. Our previous investigations have shown that the PHU-N2 network is too brittle, while the PHU-N3 network is too soft, both of them being unable to form self-standing SPE membranes for further use in batteries without the need for a separator [25]. Therefore, PHU-N2N3 mixed networks have been considered, and the best compromise was found for a N2/N3 1:3 mol mol^{-1} composition. The loading of passive filler was not attempted beyond 20wt.% due to dissolution constraint and macroscopically observed particle aggregation (see Figure S2 and Table S1).

From a chemical point of view, both approaches lead to CPEs with rather similar functional groups, i.e., the same SiO_2 passive fillers, LiTFSI salt, PEO segments, and CSBO. The main difference is that most of the CC rings of CSBO have been transformed into hydroxyurethane groups to form the cross-linking nodes of the PHU network in the second approach. However, from a topological point of view, the situation is quite different for both systems, i.e., a simple blend based on a linear polymer in the first approach and a polymer network in the second one. The aim of this contribution is to elucidate what is the best approach (simple blends or PHU networks) to obtain CPEs with optimum performance for application in a lithium battery, all other parameters being kept almost constant.

3.2. | FOURIER TRANSFORM INFRA-RED SPECTROSCOPY

The investigated CPEs with and without LiTFSI were subjected to FTIR spectroscopy (Figure 1). As far as CSBO-PEO and CSBO-PEO-SiO_2 samples are concerned, the CC rings of CSBO did not react with the hydroxyl end-group of PEO, as evidenced from the signal at ≈1798 cm^{-1} for the carbonyl of CC (Figure 1a). While the ester signal of CSBO was retained at ≈ 1740 cm^{-1} with almost no shift in both CSBO-PEO and CSBO-PEO-SiO_2 samples, as shown in Figure 1a. The contribution from C-O stretching and Si-O-Si unit bands is detected in the CPE samples with PEO and SiO_2 in the range of 1050–1100 cm^{-1}. Other characteristic bands from PEO in the region of 1000-800 cm^{-1} have also been observed in all samples, in addition to a band at ≈ 462 cm^{-1} for -O-Si in CPE samples. In Figure 1b, the comparative FTIR spectra

Published in : Macromolecular Chemistry and Physics (2025), vol. 226, n°21, e00242
DOI: 10.1002/macp.202500242
Status : Postprint (Author's version)

of CPEs are presented with increasing concentration of SiO_2 in the presence of LiTFSI. With SiO_2 (wt.%) increment, the intensity of the carbonyl band from both CC ring and ester decreased while Si-O signals (around 1180 and 462 cm^{-1}) increased in 10 to 30wt.% SiO_2-loaded CPEs. The SO_2 asymmetric stretching was observed at 1182 cm^{-1} confirming the presence of LiTFSI in all CPE samples [26, 27].

For the FTIR analysis of PHU-N2N3 CPEs, we observed almost the disappearance of the signal at 1796 cm^{-1} corresponding to CCs from CSBO and the appearance of urethane characteristic bands around 1695–1697 cm^{-1} and 1712–1716 cm^{-1} (Figure 1c). However, the weak band at 1800 cm^{-1} highlights the presence of a few unreacted CCs from CSBO in the PHU-N2N3 CPEs. Indeed, the Lewis acid-base interaction of CC and SiO_2 might offer steric hindrance for aminolysis with PEGTA, resulting in incomplete ring opening. The ester band of CSBO was observed in all samples around 1738 cm^{-1}. The remaining characteristic signalsfromPHU-N2N3anditscompositewithSiO_2 weresimilar, such as –N-H and C-N stretching around 1534–1535 cm^{-1} and 1250–1275 cm^{-1}, respectively. The characteristic signal of -Si-O was measured around ≈ 467 cm^{-1} in the composite, while the Si-O-Si signal, supposed to be around 1100 cm^{-1} could not be separated from the overlap with other organic functional groups. The dissolution of LiTFSI salt was confirmed by the observation of the SO_2 asymmetric stretching at ≈1180 cm^{-1}.

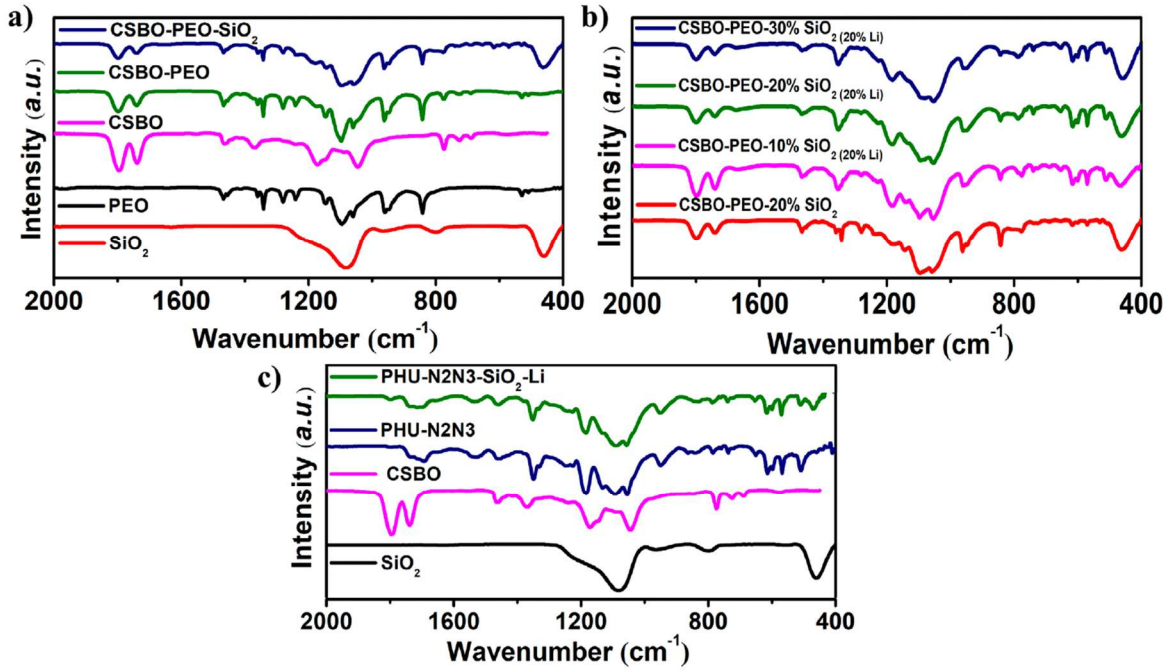

FIGURE 1 | Comparative FTIR spectra of CPEs (a) CSBO-PEO-SiO_2 in relative to blend with filler and monomers; (b) CSBO-PEO-x wt.%SiO_2 with and without LiTFSI, respectively; and (c) FTIR of PHU-N2N3 with and without SiO_2 (PHU-N2N3-SiO_2-Li containing 20wt.% LiTFSI).

Published in : Macromolecular Chemistry and Physics (2025), vol. 226, n°21, e00242
DOI: 10.1002/macp.202500242
Status : Postprint (Author's version)

3.3. THERMAL MEASUREMENTS

Differential scanning calorimetry has been performed to measure the glass transition (T_g), melting temperature (T_m), and crystallization temperature (T_c) of the investigated polymers and composites. Without added LiTFSI, T_g could not be detected while T_m was measured at 62.8°C (81%), 62.7°C (63%) and 59.4°C (58%) for PEO, CSBO-PEO and CSBO-PEO-SiO_2 (corresponding degree of crystallization χ_c of PEO segments is indicated in parentheses after each T_m), respectively (Figure 2a). Addition of LiTFSI resulted in a decrease in T_m for the composite samples (compare CSBO-PEO-20%SiO_2 with or without LiTFSI in Figure 2a), while a further decrease in T_m and χ_c was witnessed with increasing the loading in SiO_2 for the same concentration of LiTFSI. Indeed, the CPEs with LITFSI show a decrease in T_m to 48.9°C (42%), 43.7°C (37%), and 38.5°C (25%) from 10 to 30wt.% of SiO_2 as shown in Figure 2a (corresponding degree of crystallization χ_c of PEO segments is indicated in parenthesis after each T_m). The addition of SiO_2 and LiTFSI decreased the crystallinity of PEO chains in the composite, as already reported in the literature [28]. The T_g was also decreasing for these CPEs and was marked at −49.2°C, −46.3°C, and −44.8°C in order of decreasing SiO_2 content for a constant 20wt.% LiTFSI demonstrating the plasticizing effect of LiTFSI on PEO chains. Cold crystallization was also observed in all three samples with LiTFSI around 20°C between T_g and T_m, possibly due to rearrangements in the chains.

The thermal behavior of PHU network-based CPEs is substantially different. The PEGTA reference precursor shows welldefined T_m and T_c at 50.1°C and 20.1°C, respectively, as indicated in Figure 2b. While the addition of LiTFSI and SiO_2 results in a fully amorphous material with only a T_g observed for PHU-N2N3 and PHU-N2N3-SiO_2. However, no significant shift in T_g was measured on the addition of filler, i.e., −40.7°C and −40.2°C for PHU-N2N3 CPEs with and without SiO_2, respectively.

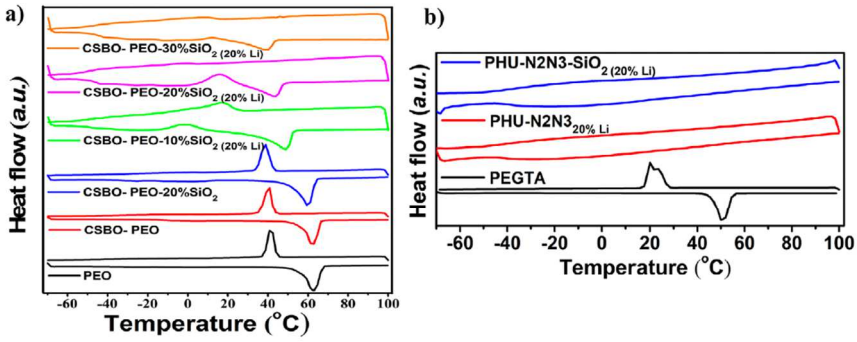

FIGURE 2 | DSC thermograms (a) CSBO-PEO-x wt.%SiO_2 with CBSO-PEO and PEO, with (20 wt.%) or without added LiTFSI; and (b) PHU-N2N3 loaded with LiTFSI (20 wt.%) with and without SiO_2 in comparison to PEGTA.

TGA was performed in the temperature range of 30°C –600°C to analyze the degradation of polymers and confirm the experimental weight% of filler. The TGA curves are shown in Figure 3a for composites with and without LiTFSI, and in comparison to PEO and CSBO-PEO.

The minor loss in weight around 100°C can be credited to the absorbed moisture in samples. In the case of PEO and CSBO-PEO, one minor degradation occurs at ≈ 246°C. While the major degradation starts at ca. 310°C with a maximum at ≈ 420°C for CSBO-PEO and CSBO-PEO-SiO_2. The LiTFSI-loaded CPE

Published in : Macromolecular Chemistry and Physics (2025), vol. 226, n°21, e00242
DOI: 10.1002/macp.202500242
Status : Postprint (Author's version)

demonstrated higher stability with degradation ranging in region 450°C, while no other degradation was observed in CPEs without salt. Total weight loss up to 80% confirmed the ≈ 20% of SiO_2 in the composite without LiTFSI. PHU networks undergo complex multiple-phase degradations due to their various functional groups, as shown in Figure 3b.

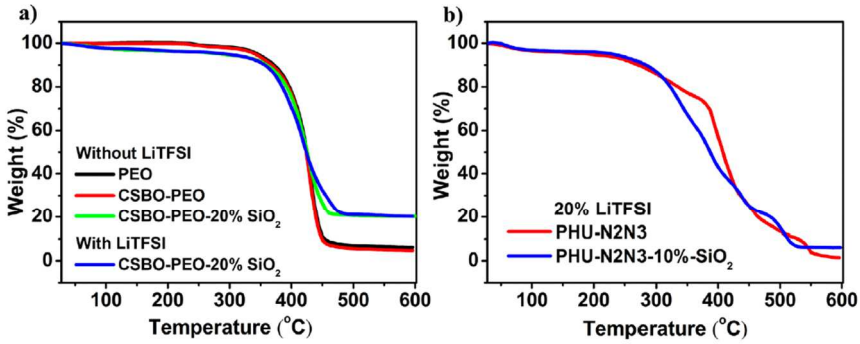

FIGURE 3 | Thermogravimetric analysis of (a) CSBO-PEO-SiO_2 compared to PEO and CSBO-PEO; and (b) PHU-N2N3-SiO_2 with and without LiTFSI, respectively.

3.4. IONIC CONDUCTIVITY

Cells assembled with CPE films in coin cells setup were subjected to potentiostatic electrical impedance spectroscopy (PEIS) for conductivity measurements at various temperatures in symmetric blocking cells with stainless steel electrodes. The conductivity (σ) was obtained by using bulk electrolyte resistance from the Nyquist plots by employing a conductivity equation involving the area and thickness of the films. Figure 4a shows the Arrhenius plot for temperature-dependent conductivity for the CSBO-PEO CPEs with 20wt.% LiTFSI and variable SiO_2 loading. The ionic conductivity ranged in the order of 10^{-6} to 10^{-4} S cm^{-1} within 20–80°C. The highest conductivity was recorded for the CPE with 10wt.% SiO_2 i.e. 7.68×10^{-6} S cm^{-1} and 3.98×10^{-4} S cm^{-1} in comparison to 3.29×10^{-6} S cm^{-1} and 2.59×10^{-4} S cm^{-1} for pristine CSBO-PEO at 20 and 80°C, respectively. The macroscopic appearance of both electrolyte films with 10wt.% and 0% SiO_2 appeared the same, with higher softness compared to CPEs with > 10wt.% SiO_2. For 20wt.% SiO_2 filler, the film demonstrated nonsticky handling, while at 30wt.% SiO_2, the CPE membrane appeared brittle and showed cracks at RT. Therefore, the conductivity values for the 30wt.% SiO_2 sample are questionable. Nevertheless, a general trend in increasing conductivity was observed with decreasing SiO_2 loading and softness.

Published in : Macromolecular Chemistry and Physics (2025), vol. 226, n°21, e00242
DOI: 10.1002/macp.202500242
Status : Postprint (Author's version)

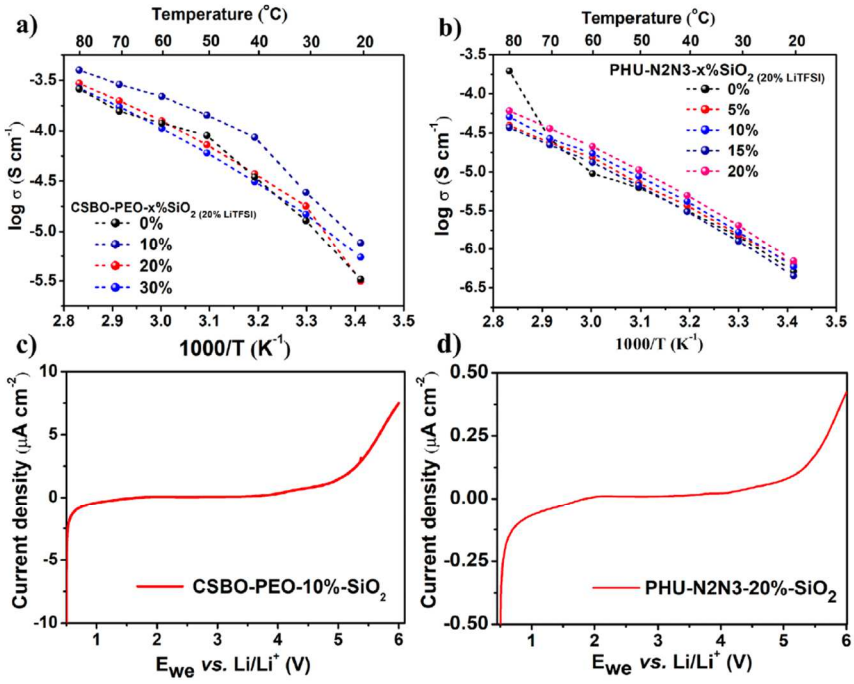

FIGURE 4 | Temperature-dependent ionic conductivity for CPEs with 20wt.% LiTFSI: (a) 0–30 wt.% of SiO_2 in CSBO-PEO-SiO_2; and (b) 0–20 wt.% of SiO_2 in PHU-N2N3-SiO_2. Linear sweep voltammetry: (c) CSBO-PEO-10%-SiO_2; and (d) PHU-N2N3%–20%-SiO_2 at 60°C.

The ionic conductivities of pristine PHU-N2N3 and the related composite,both loaded with 20wt.% LiTFSI has been investigated at various temperatures. On employing the Arrhenius model for variable conductivity, it depicted a higher conductivity of 7.01×10^{-7} S cm^{-1} for 20wt.% SiO_2 compared to 4.5×10^{-7} S cm^{-1} for PHU-N2N3 at 20°C (Figure 4b). However, a linear increase in conductivity with a similar slope could be recorded for both electrolytes. At 60°C, the CPE with 20wt.% SiO_2 delivered a conductivity of 2.13×10^{-5} S cm^{-1} while only 9.54×10^{-6} S cm^{-1} were measured for the corresponding PHU-N2N3. The reason for superior conductivity in the presence of SiO_2 filler can be credited to decreased crystallinity in the network. It can also be recalled that the PHU composite comprises unreacted CC rings, boasting Lewis acid-base interactions within the polymer network and filler particles. That could also explain the slight improvement in the conductivity due to filler addition in the network. The VFT behavior within CPE has also been investigated by considering the glass transition temperature as depicted in Figure S3. As far as the VFT model is considered, the 10 wt.% loaded SiO_2 depicted the highest conductivity with superior chain segmental motion within the electrolyte.

3.5. ELECTROCHEMICAL STABILITY WINDOW

The oxidation potential limit was investigated by LSV analysis at a slow scan rate of 0.5 mV/s. A wide electrochemical stability window(ESW)> 4.8 V versus Li/Li^+ was calculated for the CSBO-PEO-SiO_2 CPE with an aluminum cathode and lithium anode, as shown in Figure 4c. The lower decomposition of the electrolyte is credited to the addition of CSBO and SiO_2.

Published in : Macromolecular Chemistry and Physics (2025), vol. 226, n°21, e00242
DOI: 10.1002/macp.202500242
Status : Postprint (Author's version)

Similarly, a broad oxidation potential limit is achieved for the filler incorporated PHU-N2N3 network, i.e., ESW of > 4.41 V versus Li/Li^+ (Figure 4d), contrary to > 4.01 V for PHU without filler at 60°C. The presence of filler reduced the electrolyte reactivity, possibly due to the acid-base interactions between the filler surface and functional groups of the polymer chains, which are reactive to lithium metal. As a result, the SiO_2-loaded PHU electrolytes can proffer good compatibility with high-voltage cathode operation.

3.6. STRIPPING/PLATING AND TRANSFERENCE NUMBERS

The exhaustive time-dependent charge–discharge with a symmetric lithium cell was performed for more than 600+ cycles (1200 h+) with the investigated CPEs. The voltage profile with time has been depicted in Figure 5 for the PHU-N2N3%–20%-SiO_2 to highlight the kinetic hindrances, polarization, and resistance of the CPE during lithium transport. With a cut-off potential of ±2V for the first 45 cycles, the cell was run at the current density of 0.84 µA cm^{-2}. It recorded the overpotential of ~ 85 mV and ~124 mV at the first cycle and the 45th cycle, respectively. Subsequently, a drastic increment from ~376 mV was witnessed from the 46th cycle onward, reaching a cut-off voltage of +2 V at the 75th cycle. Thereafter, stabilization in output voltage was observed, which decreased from ~410 mV (at ~76th cycle) to ~ 200 mV (at ~500th cycle). This improvement in the mobility of lithium ions could be credited to the favorable morphology change and beneficial decomposition of the electrolyte over long cycling. The inset in the plot indicates the corresponding evolution in the potential for the first five cycles, the 95th -100th and 500th to 505th cycles, respectively, without much change in the plateau of stripping and plating. To understand the decomposition at the surface, XPS analysis has been performed on the electrode and electrolyte surface post-cycling, as highlighted in a further section. It can be speculated that, with higher conductivity, the PHU-N2N3-SiO_2 can prove to be an interesting candidate for full lithium-metal batteries. Similar analysis for CSBO-PEO-SiO_2 based CPE has been performed and essentially shows similar results as the PHU-N2N3-SiO_2 system.

Published in : Macromolecular Chemistry and Physics (2025), vol. 226, n°21, e00242
DOI: 10.1002/macp.202500242
Status : Postprint (Author's version)

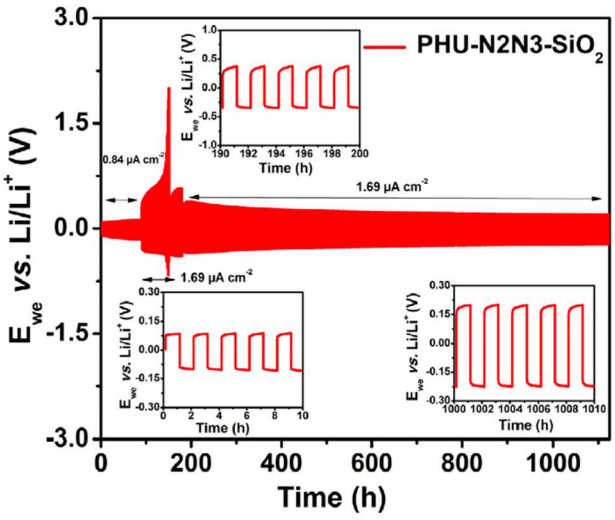

FIGURE 5 | Galvanostatic charge–discharge voltage profile for stripping-plating at various current densities at 60°C with Li|PHU-N2N3%–20%-SiO_2-CPE|Li symmetric cells with magnified plots at respective time demonstrating the constant overpotential in the inset.

3.7. LI-METAL BATTERY PROTOTYPES

Because the CSBO-PEO-SiO_2 CPE showed more interesting features than the PHU-N2N3-SiO_2 one in terms of ionic conductivity and ESW, battery prototypes based on Li-$LiFePO_4$ electrodes and CSBO-PEO-SiO_2 CPE were only considered for further detailed investigation. Those ones were subjected to constant current cycling using the GCPL technique in the range of 2–4 V at 60°C. At 0.1C, the Li|CSBO-PEO -SiO_2-CPE|LFP (20 wt.% LiTFSI and 20 wt.% SiO_2 in the CPE) cell delivered the discharge capacity of ~140 mAh g^{-1} with ~56 mV of polarization recorded in the fifth cycle, as shown in Figure 6a. On further cycling, the capacity fading was observed to approximately 104, 68, and 52 mAh g^{-1} with polarization of 77, 105, and 126 mV in respective 55th, 200th, and 300th cycles. The same cell was cycled with a variable current rate (C-rate) before long-term cycling at 0.1C. As a result, huge polarization was observed, i.e. from ca. 47 to 358 mV (along 0.1C to 2C) in subsequent charge–discharge with recorded discharge capacity of 146, 120, 65, 37, and 18 mAh g^{-1} at 0.1C, 0.2C, 0.5C, 1C and 2C, respectively as highlighted in Figure 6b. Upon further cycling at 0.1C, the cell underwent huge capacity loss as observed in Figure 6c. This could be due to sluggish kinetics of Li-ion mobility at higher current density.

Focusing on the rate capability, there was a clear loss in capacity and regain at 0.1C with not-so-promising coulombic efficiency as observed in Figure 6d.However,the electrochemical performance can be improved with further optimizations, an understanding of the interface, and electrolyte-electrode compatibility aligned with battery measurements. The post-mortem analysis on the Li-anode surface is presented in the following section to analyze the decomposed species as a result of long cycling.

Published in : Macromolecular Chemistry and Physics (2025), vol. 226, n°21, e00242
DOI: 10.1002/macp.202500242
Status : Postprint (Author's version)

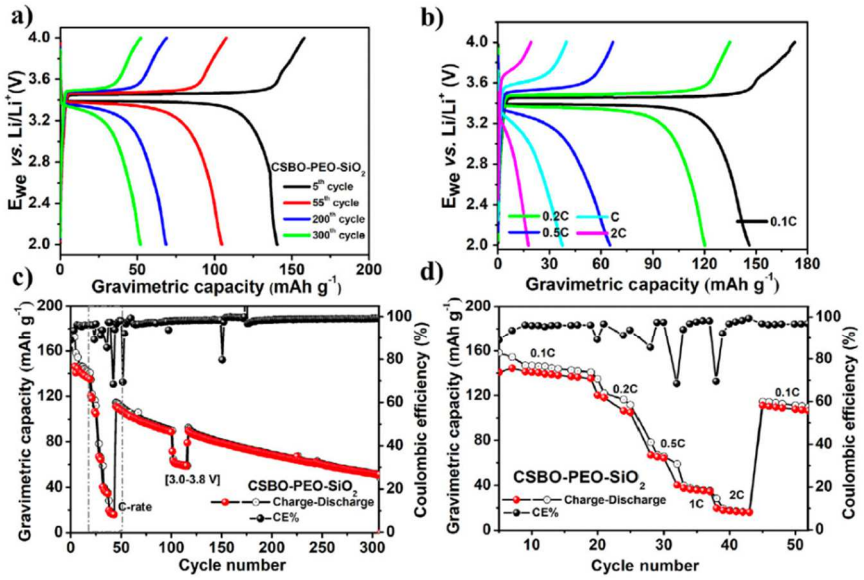

FIGURE 6 | Galvanostatic charge–discharge voltage profiles, (a) gravimetric capacity at 0.1C for respective cycles; (b) gravimetric capacity at variable current densities; (c) global capacity retention plot with cycle number; and (d) rate capability plot for Li|CSBO-PEO-SiO_2-CPE|LFP (20 wt.% LiTFSI and 20 wt.% SiO_2 in the CPE) at 60°C, respectively.

3.8. POST-MORTEM XPS ANALYSIS

The surface element characterization via XPS on the Li-anode surface from Li|CSBO-PEO-SiO_2 CPE|LFP cell cycled for more than 300+ cycles at 60°C was performed with survey spectra provided in Figure S2a and HR-XPS spectra depicted in Figure 7. The C 1s peak at 284.8 eV was used as a reference to calibrate the binding energy. In the respective HR-XPS of C1s represented in Figure 7a, we found only three distinct contributions: C-C/CH, a broad signal from O-C-O/C═O and lithium carbonate, and M-C_x corresponding to 284.8, 287.8, and 283 eV, respectively. The M-C_x signal could result from exhaustive cycling for more than 300+ cycles at variable current density, which might lead to the formation of lithium carbide in traces at the anode interface. The lithium species-containing SEI has been confirmed by the decomposition of Li 1s spectra, highlighting the formation of Li_2CO_3, LiOH, Li_2O, and Li at the binding energies (B.E.) of 55.1, 54.4, 53.7, and 52.9 eV, respectively (Figure 7b). As a result of the decomposition of LiTFSI (Figure 7c), the LiF signal has been obtained at 685.1 eV while the -CF_3 signal is recorded at 688.5 eV. This has been further evidenced from HR-XPS of S2p with LiTFSI species featuring -CF_3-SO_2, $SO_3 2^-$, SO_x, and Li_xS_y at 168.5, 166.4, 162.8, and 160.3 eV, respectively, as recorded in Figure 7d. The Li_xS_y signal indicates a relatively higher degree of salt decomposition. HR-XPS for oxygen and nitrogen can be referredtoinFigureS4b,c.Thispreliminaryanalysissuggeststhat there is an active formation of interfacial stabilization species in the Li|CSBO-PEO-SiO_2 CPE|LFP cell.

Published in : Macromolecular Chemistry and Physics (2025), vol. 226, n°21, e00242
DOI: 10.1002/macp.202500242
Status : Postprint (Author's version)

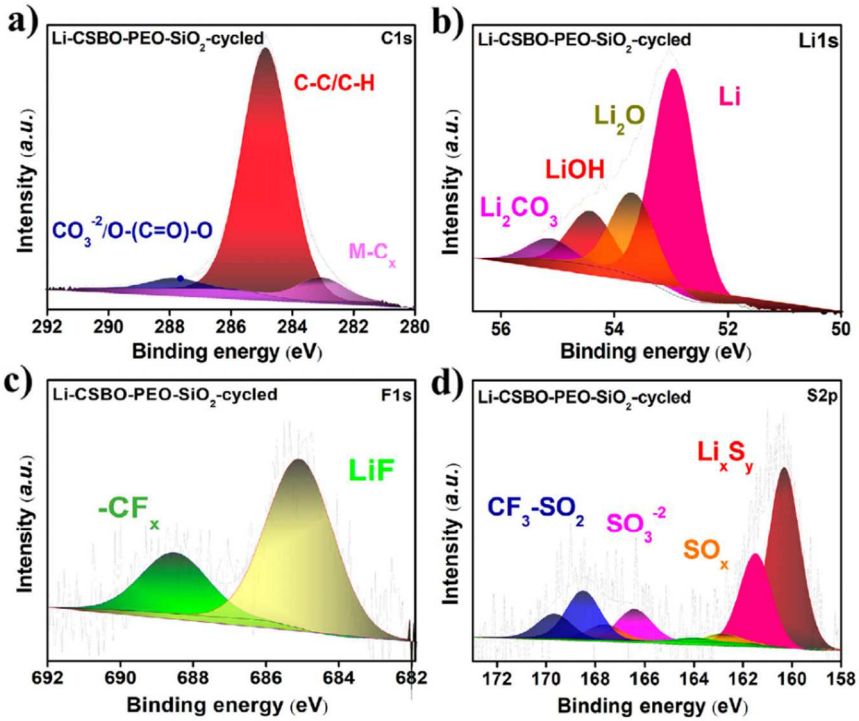

FIGURE 7 | HR-XPS of (a) carbon, (b) lithium, (c) fluorine, and (d) sulphur at the surface of the lithium anode after cycling in Li|CSBO-PEO-SiO_2 CPE|LFP cell.

4. Conclusions

Here, we attempted to investigate the combined effect of SiO_2 and polymer electrolytes and presented a comparative study. Topologically different polymers, linear chains, and networks have been used for this comparison. In both cases, the selected polymer was PEO, which was further loaded with LiTFSI to obtain the ionically conducting phase. In the case of the linear chain topology, high molar mass PEO has been used to obtain selfstanding electrolyte membranes that would not require the use of an extra separator for further electrochemical characterization. Those chains have been mixed with CSBO, a bio-sourced low molar mass molecule bearing, on average, six cyclic carbonate (CC) units. The hydroxyl end-groups of PEO were not reactive enough to ring-open the CC units of CSBO, and the latter acted as a plasticizer for PEO chains. In the case of the network topology, high molar mass PEO has been replaced by low molar mass α,ω-diamino PEO oligomers able to ring-open CC units in CSBO. A careful selection of the α,ω-diamino PEO oligomers allowed the preparation of self-standing electrolyte membranes. SiO_2 filler has been added in varying amounts to both types of CPE membranes, and lower PEO crystallinity was confirmed with the addition of SiO_2. As far as ionic conductivity is concerned, CSBO-PEO-SiO_2-based CPE demonstrated slight improvement in the conductivity, i.e., 3.98×10^{-4} S cm^{-1} while ~6.1×10^{-5} S cm^{-1} were measured for PHU-based CPEs at 80°C. To our expectations, we witnessed a broad widening in the ESW, higher for CSBO-PEO-based CPEs (> 4.8 V vs Li/Li^+) than PHU-CPEs (>4.4 vs. Li/Li^+). Furthermore, long-term charge– discharge validated CSBO-PEO-based CPEs in lithium metal

battery testing. Subsequently, surface characterizations via XPS revealed the decomposed species at the electrode and electrolyte interface. Although additional experiments should be performed for improvement, this report paved the way for efficient CPEs.

ACKNOWLEDGEMENTS

AR and JFG are grateful to INNOVIRIS for supporting this research in the frame of a BRIDGE project. CD is FRS-FNRS Research Director and thanks FNRS for financial support.

Conflicts of Interest

The authors declare no conflicts of interest.

DATA AVAILABILITY STATEMENT

The data that support the findings of this study are available from the corresponding author upon reasonable request.

References

1. A. Mauger, C. M. Julien, A. Paolella, M. Armand, and K. Zaghib,"Building Better Batteries in the Solid State: a Review," *Materials* 12 (2019): 3892.
2. N. Boaretto, I. Garbayo, S. Valiyaveettil-Sobhanraj, et al., "LithiumSolid-State Batteries: State-of-the-art and Challenges for Materials, Interfaces and Processing," *Journal of Power Sources* 502 (2021): 229919.
3. J. Kalhoff, G. G. Eshetu, D. Bresser, and S. Passerini, "Safer Electrolytes for Lithium-Ion Batteries: State of the Art and Perspectives," *Chemsuschem* 8 (2015): 2154–2175.
4. A. Manthiram, X. Yu, and S. Wang, "Lithium Battery Chemistries Enabled by Solid-State Electrolytes," *Nature Reviews Materials* 2 (2017): 16103.
5. R. Chen, Q. Li, X. Yu, L. Chen, and H. Li, "Approaching Practically Accessible Solid-State Batteries: Stability Issues Related to Solid Electrolytes and Interfaces," *Chemical Reviews* 120 (2020): 6820–6877.
6. L. Bekaert, A. Raj, J.-F. Gohy, A. Hubin, F. De Proft, and M. H. Mamme, "Assessing the Long-Term Reactivity to Achieve Compatible Electrolyte– Electrode Interfaces for Solid-State Rechargeable Lithium Batteries Using First-Principles Calculations," *The Journal of Physical Chemistry C* 126 (2022): 8227–8237.
7. A. Raj, S. Panchireddy, L. Bekaert, B. Grignard, C. Detrembleur, and J.-F. Gohy, "Solid Polymer Electrolytes with Sacrificial End Groups for a WideOxidativePotentialandStableInterfaceinLithiumMetalBatteries," *ACS Applied Materials & Interfaces* 16 (2024): 47464–47476.

8. Y.-Y. Sun, Q. Zhang, L. Yan, T.-B. Wang, and P.-Y. Hou, "A Review of Interfaces within Solid-state Electrolytes: Fundamentals, Issues and Advancements," *Chemical Engineering Journal* 437 (2022): 135179.
9. X. Zhu, K. Wang, Y. Yu, et al., "Strategies to Boost Ionic Conductivity and Interface Compatibility of Inorganic—Organic Solid Composite Electrolytes," *Energy Storage Materials* 36 (2021): 291–308.
10. J. Liang, J. Luo, Q. Sun, X. Yang, R. Li, and X. Sun, "Recent Progress on Solid-State Hybrid Electrolytes for Solid-State Lithium Batteries," *Energy Storage Materials* 21 (2019): 308–334.
11. X. Fu, D. Yu, J. Zhou, et al., "Inorganic and Organic Hybrid Solid Electrolytes for Lithium-Ion Batteries," *Cryst Eng Comm* 18 (2016): 4236– 4258.
12. M. Armand, "Polymers with Ionic Conductivity," *Advanced Materials* 2 (1990): 278–286.
13. H. Yang and N. Wu, "Ionic Conductivity and Ion Transport Mechanisms of Solid-state Lithium-Ion Battery Electrolytes: a Review," *Energy Science & Engineering* 10 (2022): 1643–1671.
14. J. Fu, Z. Li, X. Zhou, and X. Guo, "Ion Transport in Composite Polymer Electrolytes," *Materials Advances* 3 (2022): 3809–3819.
15. B. Zhang, R. Tan, L. Yang, et al., "Mechanisms and Properties of Ion transport in Inorganic Solid Electrolytes," *Energy Storage Materials* 10 (2018): 139–159.
16. M. A. K. Lakshman Dissanayake, "Nano-Composite Solid Polymer Electrolytes for Solid State Ionic Devices," *Ionics* 10 (2004): 221–225.
17. C.-W. Nan, L. Fan, Y. Lin, and Q. Cai, "Enhanced Ionic Conductivity of Polymer Electrolytes Containing NanocompositeSiO2Particles,"*Physical Review Letters* 91 (2003): 266104.
18. D. Lin, W. Liu, Y. Liu, et al., "High Ionic Conductivity of Composite Solid Polymer Electrolyte via In Situ Synthesis of Monodispersed SiO2 Nanospheres in Poly(ethylene oxide)," *Nano Letters* 16 (2016): 459–465.
19. D. Lin, P. Y. Yuen, Y. Liu, et al., "A Silica-Aerogel-Reinforced Composite Polymer Electrolyte with High Ionic Conductivity and High Modulus," *Advanced Materials* 30 (2018): 1802661.
20. S. Liu, H. Shan, S. Xia, J. Yan, J. Yu, and B. Ding, "Polymer Template Synthesis of Flexible SiO2 Nanofibers to Upgrade Composite Electrolytes," *ACS Applied Materials & Interfaces* 12 (2020): 31439–31447.
21. W.-K. Shin, J. Cho, A. G. Kannan, Y.-S. Lee, and D.-W. Kim, "Cross-linked Composite Gel Polymer Electrolyte Using Mesoporous Methacrylate-functionalizedSiO2NanoparticlesforLithium-ionPolymer Batteries," *Scientific Reports* 6 (2016): 26332.
22. J. Tu, K. Wu, J. Jiang, et al., "A Novel Ceramic/Polyurethane Composite Solid Polymer Electrolyte for High Lithium Batteries," *Ionics* 27 (2021): 569–575.
23. S. Panchireddy, J. M. Thomassin, B. Grignard, et al., "Reinforced Poly(hydroxyurethane) Thermosets as High Performance Adhesives for Aluminum Substrates," *Polymer Chemistry* 8 (2017): 5897–5909.
24. A. Raj, B. Grignard, C. Detrembleur, and J.-F. Gohy, "Solid Polymer Electrolytes Based on Poly(ethylene oxide)/Carbonated Soybean Oil Blends," *ACS Applied Polymer Materials* 7 (2025): 3033–3042.

25. A. Raj, B. Grignard, C. Detrembleur, and J.-F. Gohy, "Non-Isocyanate Poly(hydroxyurethane)-Based Networks as Solid Polymer Electrolytes for Lithium Metal Batteries," *Chemsuschem* 18 (2025): 202500007.
26. I. Rey, J. C. Lassègues, J. Grondin, and L. Servant, "Infrared andRaman Study of the PEO-LiTFSI Polymer Electrolyte," *Electrochimica Acta* 43 (1998): 1505–1510.
27. D. H. C. Wong, A. Vitale, D. Devaux, et al., "Phase Behavior and Electrochemical Characterization of Blends of Perfluoropolyether, Poly(ethylene glycol), and a Lithium Salt," *Chemistry of Materials* 27 (2015): 597–603.
28. Z. Zhang, X. Wang, X. Li, et al., "Review on Composite Solid Electrolytes for Solid-State Lithium-Ion Batteries," *Materials Today Sustainability* 21 (2023): 100316.

SUPPORTING INFORMATION

Additional supporting information can be found online in the Supporting Information section.

Supportingfile:macp70095-sup-0001-SuppMat.docx